



Research Article

Strength Recovery Effect of Bisphenol A Epoxy Resin E44 on Rock Masses with Various Crack Widths

Yaming Zhou,^{1,2} Jianhai Zhang ,^{1,2} Ru Zhang,^{1,2} Enlong Liu ,^{1,2} Lu Wang,³
and Guoyan Zhang^{1,2}

¹State Key Laboratory of Hydraulics and Mountain River Engineering, Sichuan University, Chengdu 610065, China

²College of Water Resource & Hydropower, Sichuan University, Chengdu 610065, China

³School of Architecture & Civil Engineering, Xihua University, Chengdu 610039, China

Correspondence should be addressed to Jianhai Zhang; zhangjianhai@scu.edu.cn

Received 17 September 2022; Revised 29 November 2022; Accepted 9 December 2022; Published 5 January 2023

Academic Editor: Dawei Yin

Copyright © 2023 Yaming Zhou et al. This is an open access article distributed under the Creative Commons Attribution License, which permits unrestricted use, distribution, and reproduction in any medium, provided the original work is properly cited.

As a desirable bonding and repair material, epoxy resin combined with other materials is widely used in civil engineering, but its application in underground rock engineering is still limited compared with the wide use of cement grout. To explore and optimize the effect of room temperature-cured bisphenol A epoxy resin E44 on the strength recovery of rock samples with cracks of various widths, the uniaxial compressive strength (UCS) of epoxy resin was studied and the mass ratio of the curing agent to epoxy resin (k_{CE}) was adjusted and optimized. On this basis, the UCS of the selected epoxy resin was investigated by adding diverse amounts of ethanol so that the ratio corresponding to the repair material with better mechanical properties could be selected. Artificial cracks of various widths were filled with the optimized materials, and then, a UCS test was conducted on the repaired rock samples to evaluate the effect on strength recovery and compare it with that of ultrafine Portland cement (UPC). The results show that the UCS of epoxy resin stones increases when $k_{CE} \leq 0.25$ and decreases when $k_{CE} > 0.25$, reaching a peak of 92.41 MPa. Furthermore, as the mass ratio of ethanol to curing agent and epoxy resin (k_A) increases, the UCS increases to 94.65 MPa for $k_{CE} = 0.25$ and $k_A = 0.01$. The crack width influences the UCS of the repaired rock mass. With increasing crack width, the effect of epoxy resin on recovery continuously improves, whereas that of UPC shows the opposite trend. Compared with UPC, epoxy resin has an overwhelmingly greater effect on strength recovery. For instance, for a 3 mm-wide crack, the recovered UCS for 28 d epoxy resin is 83.48 MPa, with much larger peak strains, and the strength recovery rate (k_r) is 77.55%; however, the k_r of UPC is only 15.12%.

1. Introduction

During excavation and blasting in underground engineering, the release of in situ stress and surrounding rock deformation cause relaxation around the chamber to a certain depth, and time-dependent deformation characteristics of crack growth appear over time, which have a detrimental impact on the stability of the surrounding rock [1–4]. Figure 1 shows the cracked rock surrounding the main underground powerhouse of the Shuangjiangkou Hydro-power Station.

Over time, material performance deteriorates because of the inherent degradation of materials (such as weathering and crack expansion) [5–7] and external stress adjustment

[8], which further leads to cracking and instability of the surrounding rock, thus affecting the service performance and safety of a structure [9, 10].

In view of the above engineering problems, grouting the ruptured surrounding rock is of great interest. There are numerous grouting methods, and one of the most common methods is permeation grouting [11]. Grouting reinforcement can effectively avoid geological disasters such as water penetration and instability [12–15]; hence, grouting materials are the key factor affecting recovery [16, 17]. The repair materials involved in civil engineering include cement [18–20], ground polymers [9, 21, 22], polymer modification slurries, mortars [23], and other materials [24, 25]. Grouting can be divided into cement grouting and chemical grouting,

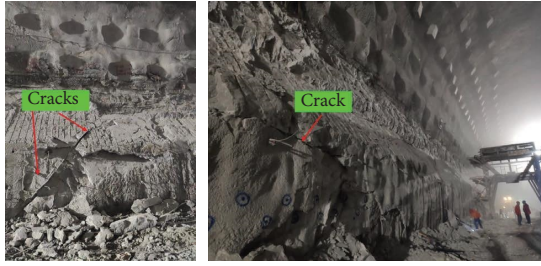


FIGURE 1: Cracked surrounding rock of the main underground plant.

or a mixture of both [23]. The chemical grouting materials mainly include polyurethane and epoxy resin. When chemical grouting is used, it can both bond the crack part and play a water-stopping role, and it is suitable for cracks with a fine width [26]. The current study on grout mainly focuses on penetrability [27–29]; however, the strength of stone is also significant. Aziz et al. [30–32] investigated the mechanical properties of grout stone bodies. Although cement is widely used in buildings, it has the disadvantages of low compressive strength, poor tensile strength, and high porosity [33]. Epoxy resin is a thermosetting material often used as a binder and for other functional materials, is often used in the military and packaging engineering industries, and is involved in civil engineering and other fields [26]. When the external stress is too large, the cement material easily breaks up, and the strength is greatly reduced. Compared with cement, epoxy resin possesses fair strength, bonding effect, and toughness characteristics and can adapt to large deformations while ensuring certain strength.

Research on epoxy resin as a repair material [34] is relatively limited due to its relatively high cost and mainly involves mixing it with other materials [23]. The surface bonding performance is also a significant index used to evaluate repair quality. For example, Axelsson and Gustafson [35] designed a direct measurement of the shear strength to determine the shear strength of cement-based injection grouts in the field. The binding between the repair materials and a substrate is generated through physical, chemical, and mechanical interactions, such as adhesion caused by newly formed gels on the bonding surface, van der Waals forces, and friction of the surface morphology [36, 37]. The adhesion strength is connected to the rock strength and surface roughness [38]. However, the effect of different crack widths on strength recovery has rarely been studied, and the UCS of repaired samples is an important index [39–41]. Li et al. [42–44] explored the influence of crack widths or quantities on grouting, but the strength of the repaired rock masses was not considered. Zhong et al. [45] carried out UCS testing on specimens with various initial crack lengths in 10 mm-wide joints, but different joint widths were not considered.

Broken rock cracks vary from subtle cracks to wide cracks, and these repaired cracks of various widths may have diverse influences on the mechanical properties of a rock mass [46]. Therefore, investigating the effect on the strength

recovery of a ruptured rock mass with diverse crack widths filled with repair grout is significant.

The physical and mechanical properties of repair materials are the main reference indices that balance them as repair materials [47–51]. Epoxy resin is mainly a type of thermosetting resin, and most thermosetting resins are viscous liquids at room temperature; their viscosity is greatly affected by temperature, and they can be cured when mixed with the corresponding curing agent. Due to the high viscosity of epoxy resin, especially during mechanical stirring in air, a large amount of air mixes into the epoxy resin in the form of bubbles. Therefore, many defects of different sizes are formed in the epoxy resin, which decrease the mechanical properties of the epoxy resin and ultimately weaken the effect on the recovery of the repaired rock. The repair grout with a lower viscosity can better fill the subtle cracks, and the working performance can also be improved, enhancing the effect on recovery. To boost fluidity, a certain amount of ethanol was added to the epoxy resin and the curing agent, and vacuum mixing was introduced to reduce the content of air.

Room temperature-cured bisphenol A epoxy resin E44 was selected as the repair material, and the viscosity of the epoxy resin material at different temperatures and ethanol contents was determined. Then, the uniaxial compressive strength (UCS) [52–54] of epoxy resin stones with different k_{CE} values was studied and compared with that of epoxy resin and ultrafine Portland cement (UPC) stones stirred in air. Furthermore, the USC of the stone bodies was studied by adding ethanol, corresponding to various k_A values. The preferred repair material components for the rock samples with cracks of various widths were then determined. Finally, a UCS test performed on repaired rock samples and scanning electron microscopy (SEM) were used to explore the changes in the mechanical properties, and the test results were analyzed and discussed, thus enriching the theory of rock strength recovery.

2. Materials and Methods

2.1. Materials and Devices

2.1.1. Epoxy Resin, Curing Agent, and Ethanol. In this study, room temperature-cured environmentally friendly bisphenol A epoxy resin E44 and epoxy curing agent 650 (condensation of fatty acids and fatty amines) produced by Hunan Licheng New Material Technology Co., Ltd. (Hunan, China) were selected. At room temperature, as shown in Figure 2, the epoxy resin adhesive (E44) is a colorless and transparent viscous liquid, and the epoxy curing agent (650) is a yellow-red viscous liquid. The density of epoxy resin is 1.13 g/ml, which is greater than that of the curing agent, approximately 0.93 g/ml. The UCS of grout with various ratios was studied. Anhydrous ethanol produced by Chengdu Jinshan Chemical Reagent Co., Ltd. (Sichuan, China) was used with a density of 0.79 g/ml. The influence of ethanol at various concentrations (0, 0.01, 0.015, and 0.02) on the viscosity and UCS of epoxy resin was explored to optimize the ratio to improve its effect on rock strength recovery.

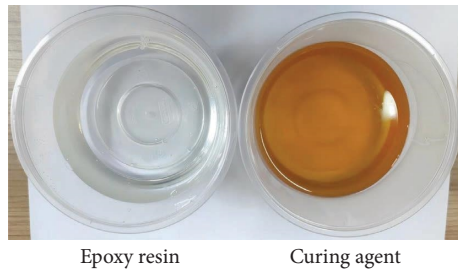


FIGURE 2: Epoxy resin and curing agent.

2.1.2. UPC and Tap Water. The UPC was produced by Shandong Kangjing New Material Technology Co., Ltd. (Shandong, China), and its particle size was approximately $7\ \mu\text{m}$. UPC is a traditional grouting material and the main grouting material for roadways, tunnels, and other projects. The cement grout had a water–cement ratio (W/C) of 0.8, and the water was from a municipal tap.

2.1.3. Self-Designed Grouting Repair Device. A schematic diagram of the self-designed grouting repair device is shown in Figure 3, which mainly consists of a bottle of liquid nitrogen with a purity of 99.2%, a pressure reduction valve, a transparent cylinder, two diversion grooves, hose clamps, rubber films, a rock sample, and a drain hole. As shown in Figure 3, the transparent cylinder is made of two halves, and the covers at both ends are made from colorless transparent Plexiglas material so that the amount and flow of grout can be clearly observed.

During the grouting repair of fractured rock samples under nitrogen pressure, the running track of the grout was as follows, as shown in Figure 4: grout in the upper cylinder \rightarrow inlet channel of the semicircular diversion groove on one side of the cylinder wall \rightarrow lower end of the crack \rightarrow rock crack \rightarrow upper end of the crack \rightarrow grout discharge channel of the semicircular diversion groove on the other side of the cylinder wall \rightarrow lower guide pipe orifice \rightarrow collection container outside the barrel.

The grouting method can effectively repair different crack samples, considering the adjustable grouting pressure, effective air outlet, convenient disassembly and installation, adjustable crack width, and visualization.

2.1.4. Schematic Diagram of the Experiment. Figure 5 shows a schematic diagram of the experimental procedures. The experiment mainly includes studies of the properties of the repair materials and the UCS of the repaired samples.

2.2. Sample Preparation

2.2.1. Vacuum Mixing and Samples. To determine the optimal mass ratio k_{CE} , epoxy resin and the curing agent at different ratios (0.125, 0.25, 0.375, 0.5, 0.75, and 1.0) were vacuum stirred, and then, ethanol at different proportions k_A (0, 0.01, 0.015, and 0.02) was added to the k_{CE} -optimized material to further enhance the UCS behavior. As shown in Figure 6, the mechanical mixing facility mainly consisted of

a vacuum pump, a barometer, a mixing rod, a sealing plug, and a flask, and mixing was carried out with the vacuum pump for 10 min. Mixing and curing were conducted at $23 \pm 2^\circ\text{C}$, the air humidity was approximately 30–40%, and the curing time was 28 d. A group of samples with a k_{CE} of 0.25 and an UPC sample with a W/C of 0.8 were selected for stirring in air for comparison. The UPC was cured for 28 d, soaked at $23 \pm 2^\circ\text{C}$ and wet cured, which was followed by natural air drying.

The epoxy resin samples are shown in Figure 7, from which different k_{CE} values are shown to result in different colors, and the larger k_{CE} is, the darker the color. In contrast, the color of the sample stirred in air is whitish yellow because of the residual air.

2.2.2. Artificial Cracks and Repair Method. Granitic rock was taken from the main underground plant of the Shuangjiangkou Hydropower Station. Its main elements are O and Si based on X-ray energy dispersive spectroscopy (EDS), as shown in Table 1.

To better explore the repair effect on rock masses with different crack widths, artificial fractures need to be prepared in laboratory tests [9, 21]. Standard rock samples of $\Phi 50 * h100$ (mm) were cut at the middle position along a line at 45° with respect to the horizontal direction [55], with a total length of 70.7 mm. The cracks along the height direction were 1 mm, 3 mm, 5 mm, and 7 mm in size. Note that the actual crack width is $1/\sqrt{2}$ times these sizes. A schematic diagram is shown in Figure 8(a).

Using the grouting repair device in Figure 3, high-pressure gas pushes the repair grout into the artificial rock crack and the formed grout stone bonds to the rock surface. After a certain amount of maintenance time, the sample is removed, the surface is polished, and a sample is then taken for UCS testing. The test results are compared with those of the intact rock sample to evaluate the effect on the recovery of different grout materials or various crack widths. A schematic diagram of a repaired sample is shown in Figure 8(b).

The artificial cracks were filled with the optimized epoxy resin material with $k_{CE} = 0.25$ and $k_A = 0.01$. A UPC with a W/C of 0.8 was selected for the comparison study, and the rock crack widths were 1 mm and 3 mm with 28 d of curing and 3 mm with 14 d of curing. The curing conditions for the samples were the same as those in Section 2.1.2.

2.3. UCS Test and Strength Recovery Ratio. The mechanical properties of grout stone bodies are significant for evaluating repair materials. Epoxy resin and UPC samples were used for UCS tests on an MTS 815 system, as shown in Figure 9. Since the epoxy resin had a large deformation relative to the granite sample, a loading rate of 2 mm/min was adopted, while for brittle samples, such as UPC, granite, and repaired samples, the chosen rate was 0.04 mm/min.

To quantify the effect on strength recovery, the strength recovery ratio k_r is defined as shown in formula (1):

$$k_r = \frac{P_r}{P_i}, \quad (1)$$

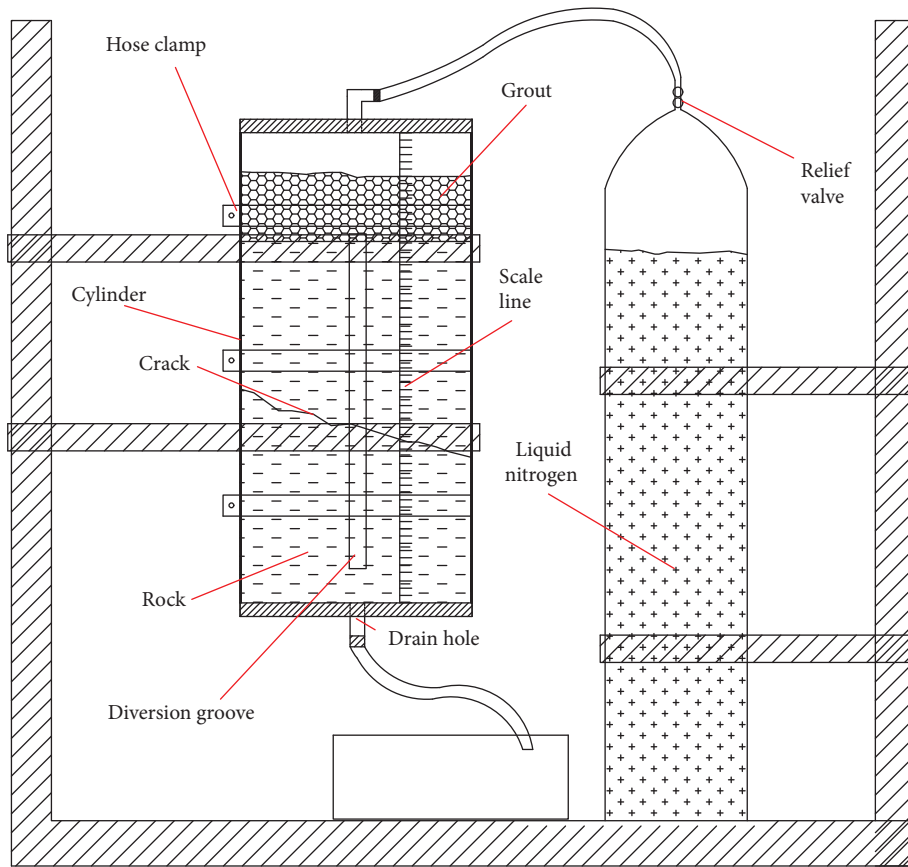


FIGURE 3: Schematic diagram of the self-designed grouting repair device.

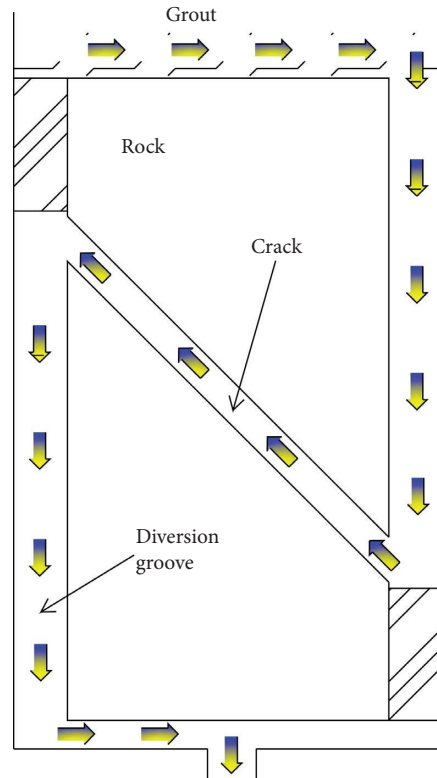


FIGURE 4: Schematic diagram of the grout filling process.

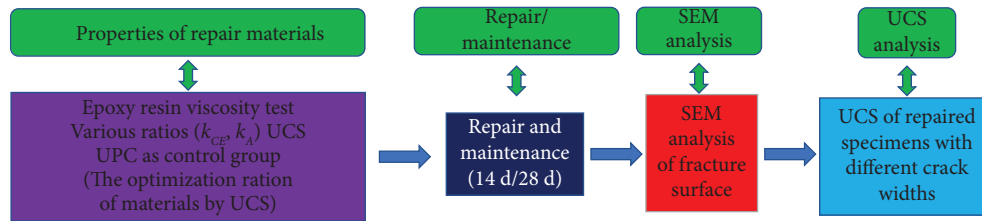


FIGURE 5: Schematic diagram of the experimental procedures.

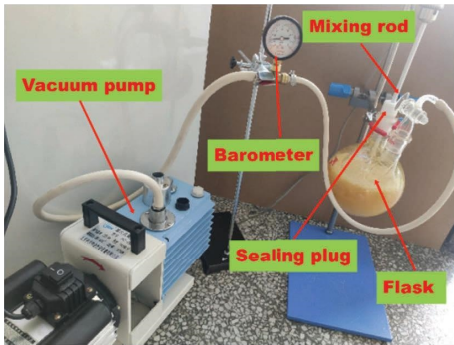


FIGURE 6: Epoxy resin mixed with a vacuum pump.

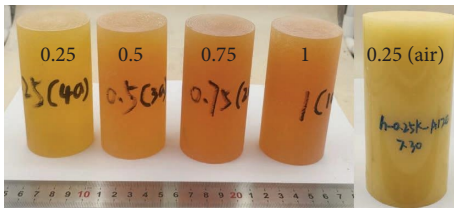


FIGURE 7: Epoxy resin samples with different k_{CE} values and a sample stirred in air.

TABLE 1: Elemental composition of the granite.

Elements	wt (%)	Atomic percent
C	4.87	8.31
O	44.53	57.05
Na	1.52	1.35
Mg	0.59	0.50
Al	6.32	4.80
Si	31.67	23.11
K	4.04	2.12
Ca	2.68	1.37
Fe	3.79	1.39
Total	100.00	100.00

where P_i is the UCS (MPa) of the intact rock and P_r is the UCS (MPa) of the repaired sample.

3. Results and Analysis

3.1. Grout Viscosity. The viscosity changes of epoxy resin with a k_{CE} of 0.25 and a k_A of 0.01 or 0.02 were tested at 20 s, 80 s, and 200 s and at 24°C and 29°C [56]. A DV-79 digital viscosity instrument was used. As shown in Figure 10, the

viscosity of the epoxy resin decreases with increasing ethanol fraction, gradually increases with time, and decreases at a higher temperature. For example, at 24°C and 20 s, the viscosities are 418 MPas, 258 MPas, and 223 MPas for resin with k_A values of 0.00, 0.01, and 0.02, respectively. At 29°C, the corresponding values change to 258 MPas, 186 MPas, and 124 MPas. With time, at 29°C and a k_A of 0.02, the measured viscosity gradually increases. At 20 s, 80 s, and 200 s, the viscosities are 124 MPas, 129 MPas, and 135 MPas, respectively.

3.2. UCS of Intact Rock Samples. The intact and damaged granite samples are shown in Figure 11. The average UCS, elastic modulus, and peak strain are 107.64 MPa, 137.23 GPa, and 0.008, respectively. The stress-strain curve is shown in Figure 12, showing typically brittle damage behavior.

3.3. UCS of Grout Stone Bodies

3.3.1. Epoxy Resin and UPC Test Samples. Figure 13 shows the compression conditions of grout stone samples with k_{CE} values of 0.25, 0.5, 0.75, 1, and 0.25 (mixed in air) and the UPC sample. Figure 14 shows the stress-strain curves of stone bodies corresponding to k_{CE} values of 0.125, 0.25, 0.375, 0.5, 0.75, and 1.00, and Figure 15 demonstrates their UCS and peak strains. The stress-strain curves for a k_{CE} of 0.25 and UPC are shown in Figure 16. The epoxy resin sample does not crack when the strain reaches 0.09 or higher, whereas the UPC and granite samples (see Figure 11) are broken at relatively small strains. For different k_{CE} values, the mechanical properties vary, and as the ratio increases, the UCS changes from small to large and then drops, with a maximum UCS value of 92.41 MPa for a k_{CE} of 0.25. The variation range of the peak strain is small, within the range of 0.0454–0.0501.

For epoxy resin, the UCS of the sample mixed in the air is smaller than that of the sample stirred in a vacuum, and the corresponding UCS values are 75.88 MPa and 92.41 MPa. The peak strain of the sample stirred in the air is significantly smaller than that stirred in a vacuum. The main reason may be that a large number of bubbles are mixed in the mixing process, resulting in more voids (see Figure 17) in the epoxy resin material, which ultimately leads to a lower UCS and peak strain. The cement sample is brittle compared with the epoxy resin, and the peak strain is significantly smaller, with the UCS being only 25.32 MPa. Comparatively speaking, epoxy material has high compressive strength and good ductility.

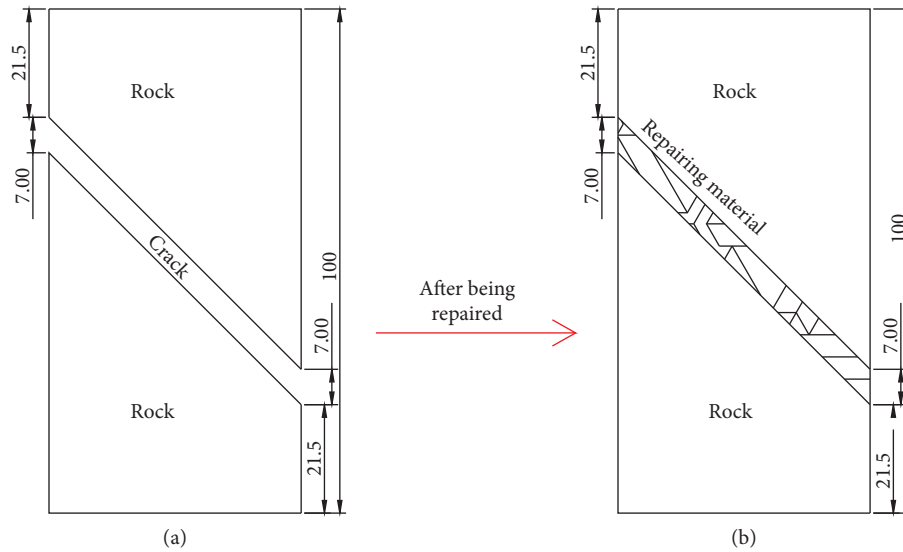


FIGURE 8: Schematic diagram of the sample (a) before repair and (b) after repair (unit: mm).

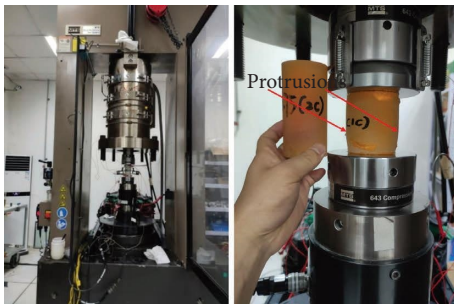


FIGURE 9: UCS tests on an MTS815 system.

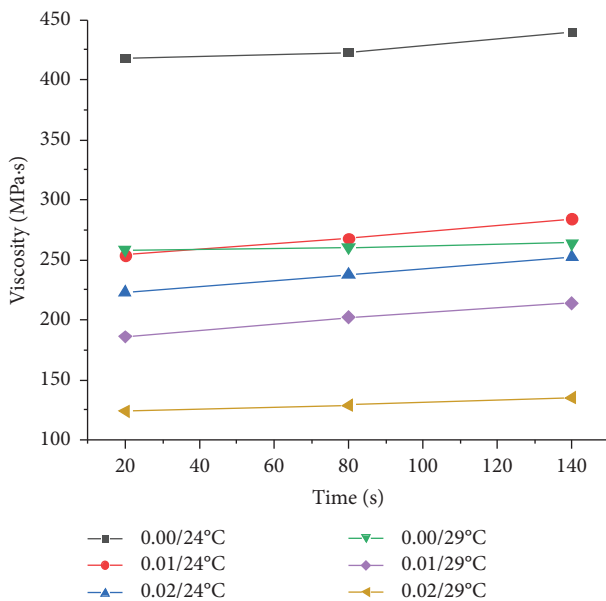


FIGURE 10: Viscosity of epoxy resin with a k_{CE} of 0.25 and a k_A of 0.01 or 0.02 at 24°C or 29°C.

3.3.2. *Epoxy Resin Samples with a k_{CE} of 0.25 and Different k_A Values.* Figure 18 shows stress-strain curves of epoxy resin samples with a k_{CE} of 0.25 and k_A values of 0, 0.01, 0.015, and 0.02. Figure 18 shows that the mechanical properties are related to k_A , and after the maximum value is reached, the stress decreases fairly slowly with long-term strain compared with that of the rock shown in Figure 12. The UCS and peak strain are shown in Figure 19, from which the UCS first increases and then decreases with increasing k_A . When k_A is 0.01, the UCS reaches a maximum value of 94.65 MPa. The peak strain gradually decreases, but the change is not obvious, within 0.0460 to 0.047. Therefore, the amount of ethanol can affect the UCS and the peak strain of the epoxy resin. Ethanol does not react with epoxy resin, and the change in UCS may be caused by the increase in fluidity and decrease in the air content of epoxy resin, resulting in an increase in UCS with more thorough mixing. However, ethanol is distributed in the epoxy resin as a single molecule, and with increasing k_A , these molecules play a certain “lubricating role”; thus, its strength gradually decreases above a certain content.

3.3.3. *Elastic Modulus and Poisson’s Ratio.* The change in the elastic modulus and Poisson’s ratio of different materials is shown in Figure 20, from which the elastic moduli are found to be different for various k_{CE} values. The elastic modulus at a k_{CE} of 0.25 is 2.78 GPa, which is larger than the elastic modulus of 2.00 GPa at a k_{CE} of 1 and smaller than the elastic modulus of 2.85 GPa at $k_{CE} = 0.25$ and $k_A = 0.01$, but they are all smaller than the elastic modulus of 4.38 GPa for UPC. The maximum elastic modulus of intact rock is 18.47 GPa, which is distinctly larger than that of the other groups. Therefore, the elastic modulus of epoxy resin is less than that of UPC, and both are significantly less than that of granite. The elastic modulus of 2.78 GPa achieved with vacuum mixing is greater than the value of 2.49 GPa achieved with mixing in the air.

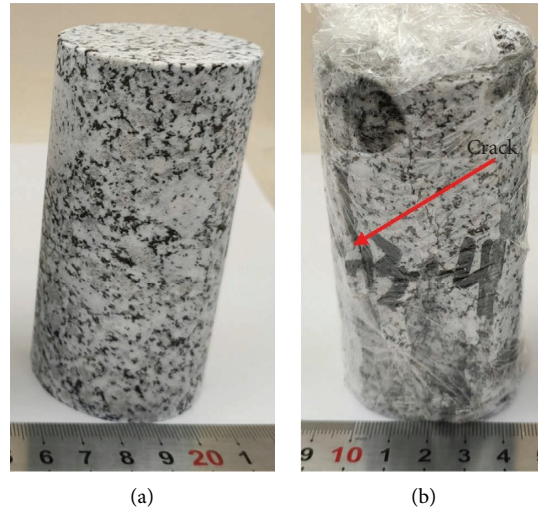


FIGURE 11: Intact and damaged rock samples.

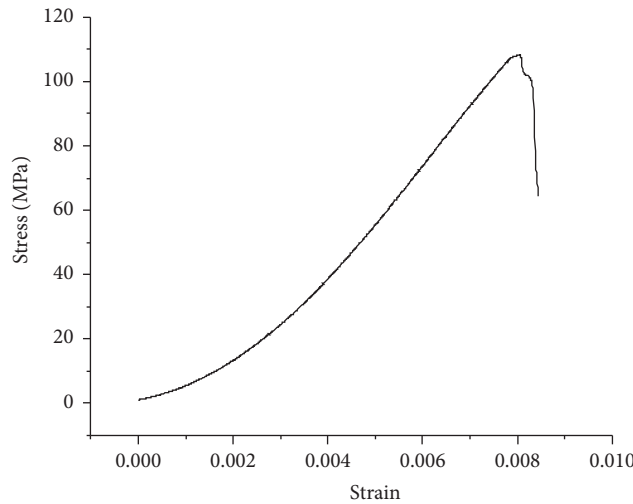


FIGURE 12: Stress-strain curve of granite samples.

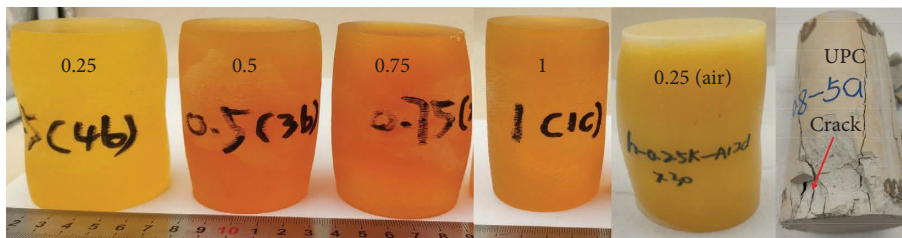


FIGURE 13: Epoxy resin after compression and broken UPC samples.

Poisson’s ratio of different materials varies, and Poisson’s ratio of epoxy resin materials is large, between 0.316 and 0.355, whereas that of UPC is 0.130. However, the smallest value is 0.113 for intact rock.

The elastic modulus of samples with different k_{CE} values is shown in Figure 21. With increasing k_{CE} , the elastic modulus has a trend of first increasing and then decreasing, reaching a maximum value of 2.78 GPa at a k_{CE} of 0.25.

Poisson’s ratio of epoxy resin first decreases and then gradually increases, ranging from 0.336 to 0.359 on a small scale. A possible reason is that these samples are all vacuum-stirred, and their mixed materials are relatively similar.

Figure 22 shows the elastic modulus and Poisson’s ratio of samples with different k_A values and a k_{CE} of 0.25. The elastic modulus of epoxy resin first increases and then decreases with increasing k_A . It reaches the maximum value of

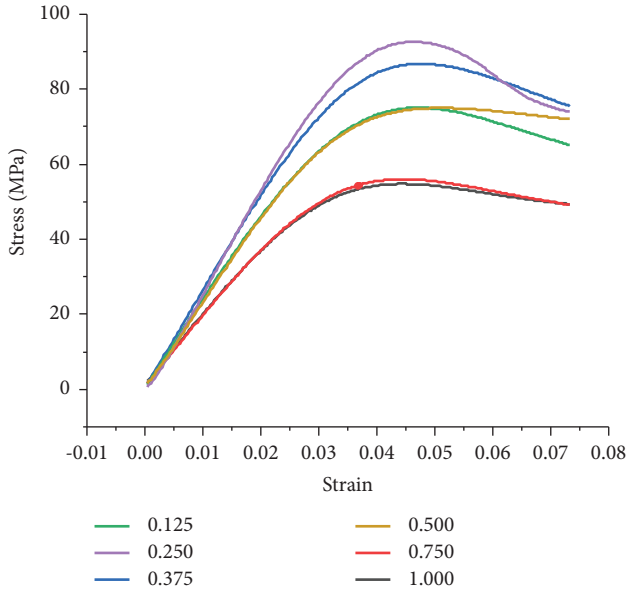


FIGURE 14: Uniaxial stress-strain curves for different k_{CE} values.

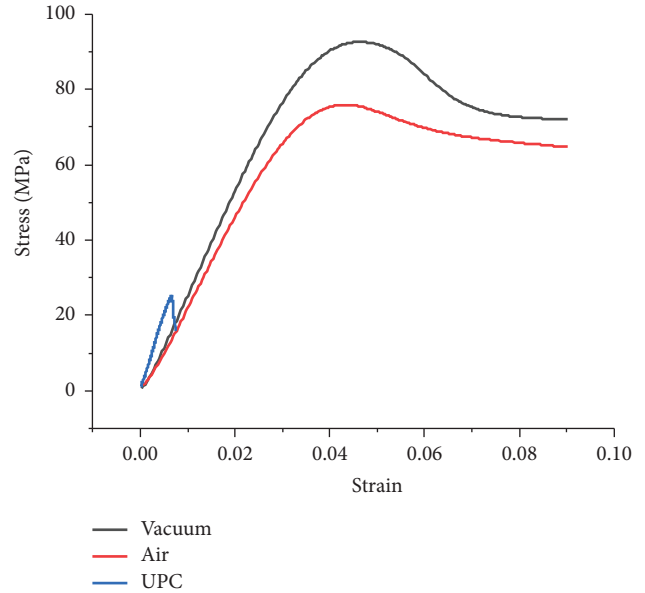


FIGURE 16: Stress-strain curve of stones with a k_{CE} of 0.25 under air or vacuum mixing conditions and that of UPC.

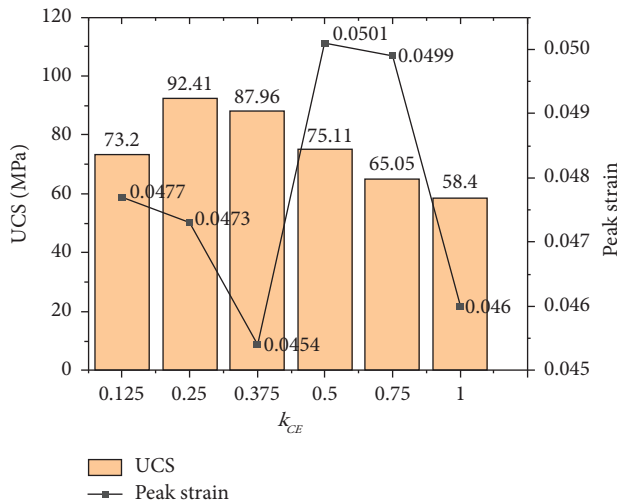


FIGURE 15: UCS and peak strain for different k_{CE} values.

2.85 GPa at a k_A of 0.01 but varies in a small range of 2.56–2.85 GPa. Poisson’s ratio changes between 0.335 and 0.340.

3.4. Strength Repair Effect Analysis

3.4.1. Repair with Epoxy Resin. The conditions before and after the failure of samples repaired with epoxy resin with a k_{CE} of 0.25 and a k_A of 0.01 are shown in Figures 23–25. Figures 23–25 show that the damage corresponds to the peeling of the adhesive interface between the rock and epoxy resin, and the surfaces of the granite and epoxy resin are relatively intact. This is mainly due to the UCS of the granite exceeding 100 MPa, and the bond strength of the repaired surface is not sufficiently large.

After 14 d of curing, with increasing repair width, the epoxy resin is completely stripped and later cracked from the surface, and the edge of the rock surface is broken. When the width is between 1 mm and 3 mm, the two epoxy resin areas on the rock surfaces are almost equal. When the repair width is between 5 mm and 7 mm, only failure of the ends occurs. At 28 d, the entire interfaces are detached for the 1 mm and 3 mm cracks, whereas only the epoxy resin-tearing phenomenon occurs for the 5 mm and 7 mm widths, in which the epoxy resin area is nearly equal to the split fracture area and is similar to that at 14 d for widths of 1 mm and 3 mm. The crack phenomenon at the end is virtually the same as that at 14 d. These phenomena mainly occur because the epoxy resin strength is still developing as the crosslinking reaction progresses, and the bond strength between epoxy and rock also increases at day 14 relative to that at day 28. With increasing axial pressure, due to bond strength development, the size effect becomes increasingly obvious [6], resulting in an increasing shear force on the epoxy resin. In general, the damage condition of the surface is mainly related to the crack width and curing time.

SEM images of the cracks under curing conditions at days 14 and 28 are shown in Figures 26 and 27, respectively. The surface of the broken rock is rough, while the surface of the epoxy resin is smooth, and there is no obvious gap in the bond surface on day 28, indicating that the bond between the epoxy resin and the rock surface is relatively strong. Compared with that observed with 14 d of curing, the rupture surface of epoxy resin observed with 28 d of curing is smoother, which may be because the epoxy resin strength is developing with the curing time.

Figure 28 shows the UCS and peak strains at days 14 and 28 with a k_{CE} of 0.25 and a k_A of 0.01. With increasing repair width, the UCS improves, and the peak strain increases. Overall, the UCS at day 28, within 80.21–93.16 MPa, is larger

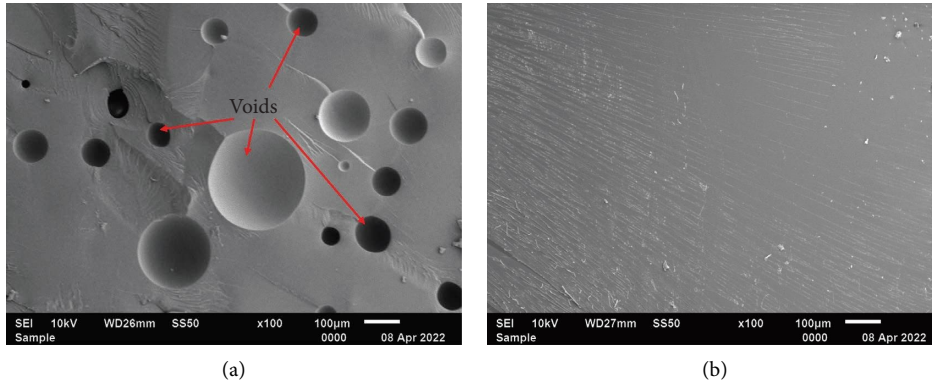


FIGURE 17: SEM image of epoxy resin samples mixed in air (a) or stirred in vacuum (b).

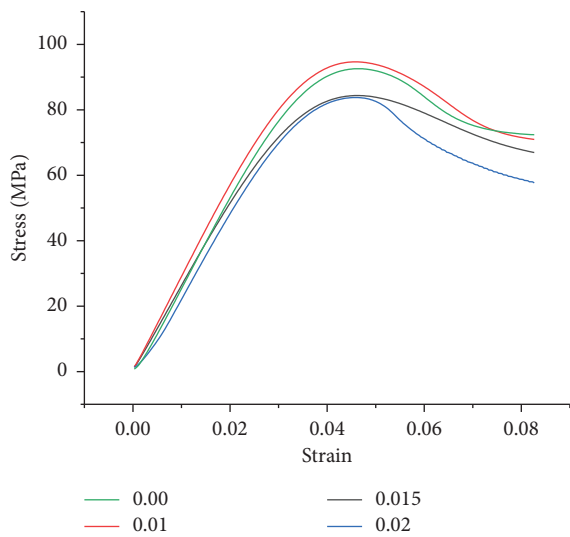


FIGURE 18: Stress-strain curves with different k_A values and a k_{CE} of 0.25.

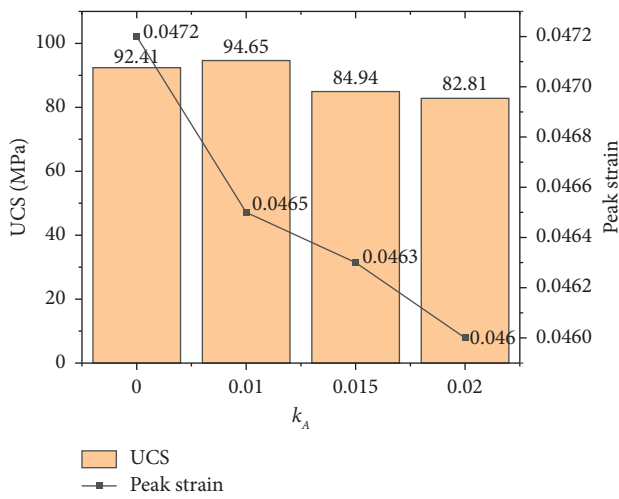


FIGURE 19: UCS and peak strain of epoxy resin with a k_{CE} of 0.25 and various k_A values.

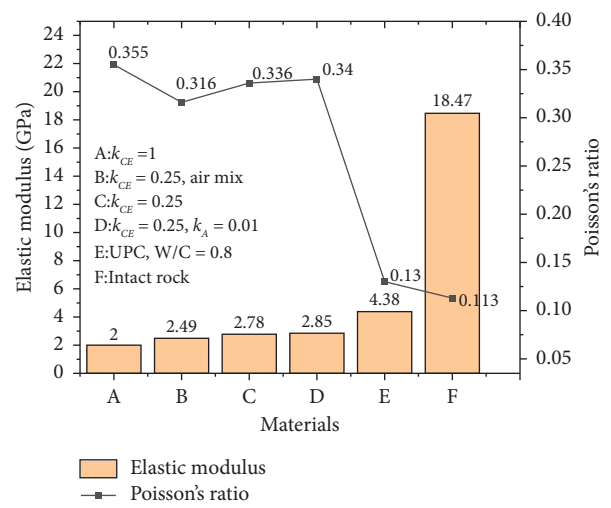


FIGURE 20: Elastic modulus and Poisson's ratio of different materials.

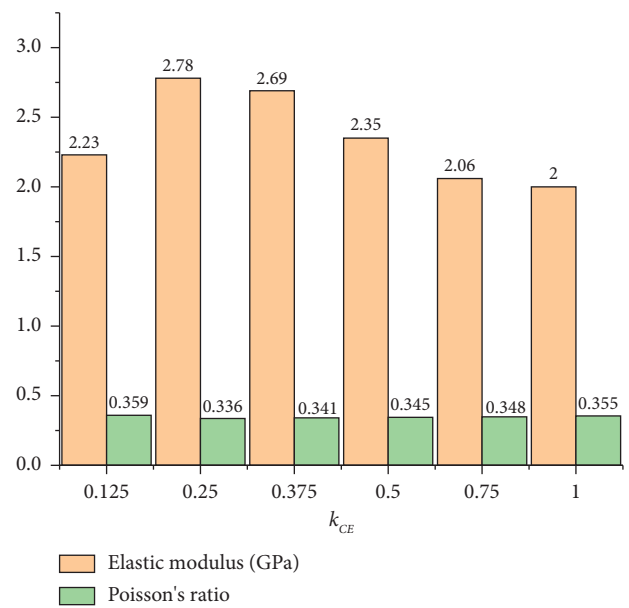


FIGURE 21: Elastic modulus and Poisson's ratio of stones with different k_{CE} values.

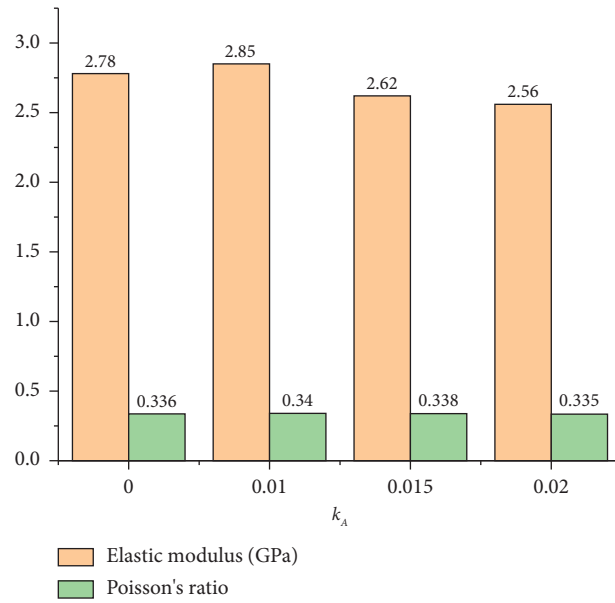


FIGURE 22: Elastic modulus and Poisson's ratio of stones with different k_A values and a k_{CE} of 0.25.

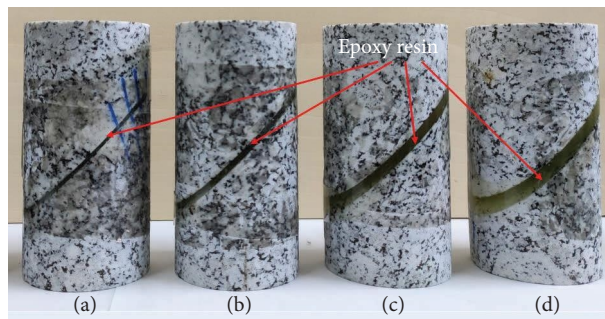


FIGURE 23: Epoxy resin-repaired samples with different repair widths (a) 1 mm; (b) 3 mm; (c) 5 mm; and (d) 7 mm before failure.

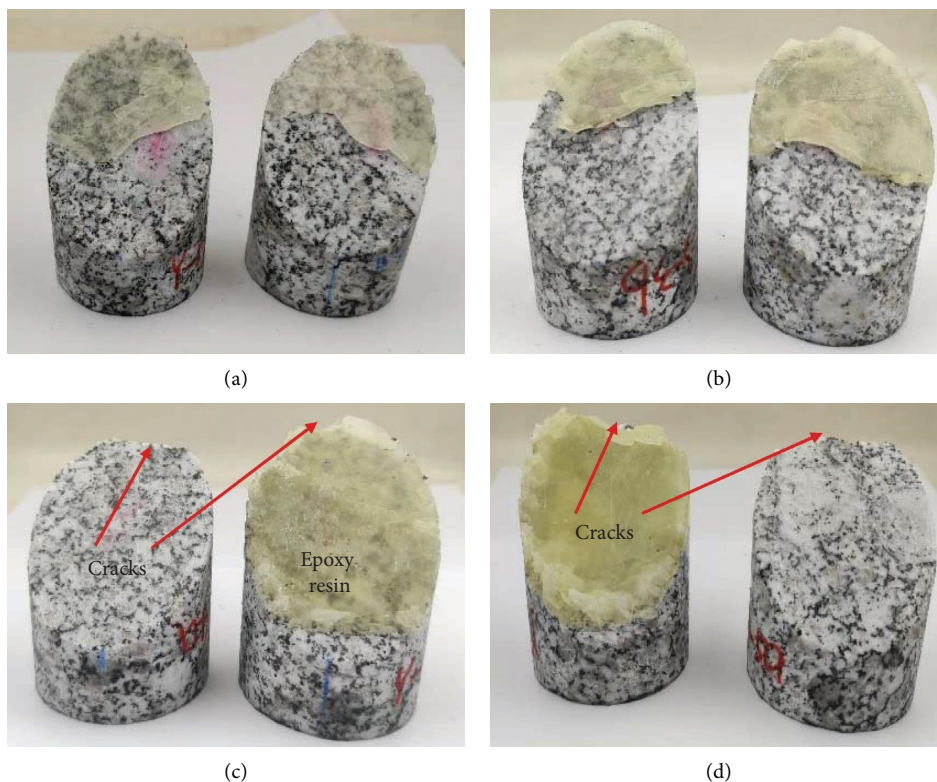


FIGURE 24: Epoxy resin repaired samples with different repair widths (a) 1 mm; (b) 3 mm; (c) 5 mm; and (d) 7 mm after failure at day 14.

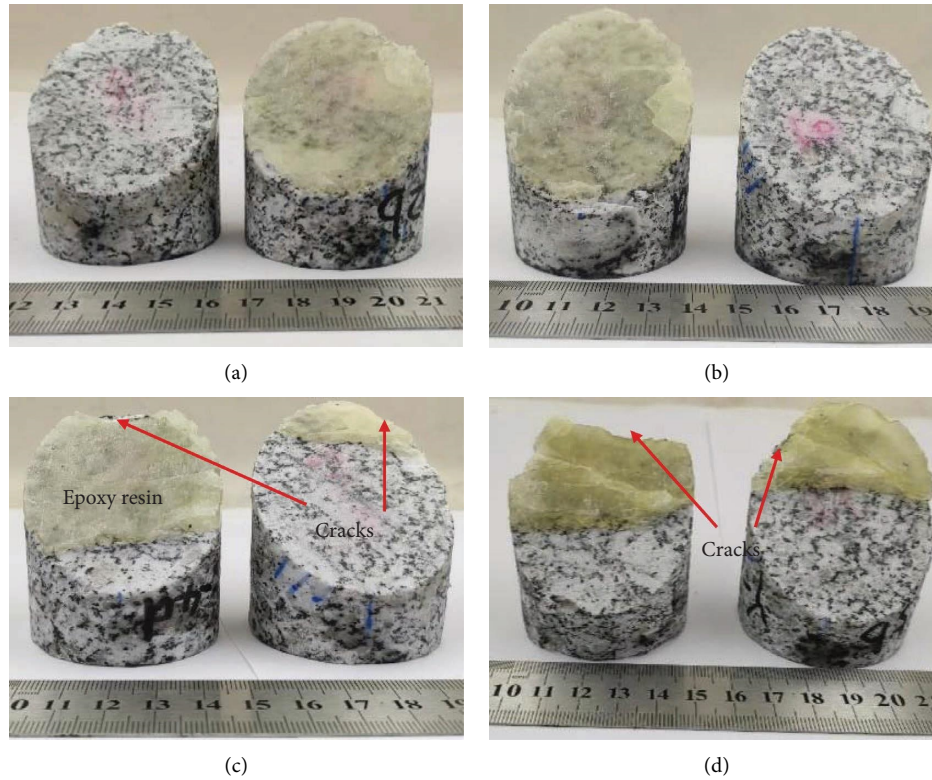


FIGURE 25: Epoxy resin-repaired samples with different repair widths (a) 1 mm; (b) 3 mm; (c) 5 mm; and (d) 7 mm after failure at day 28.

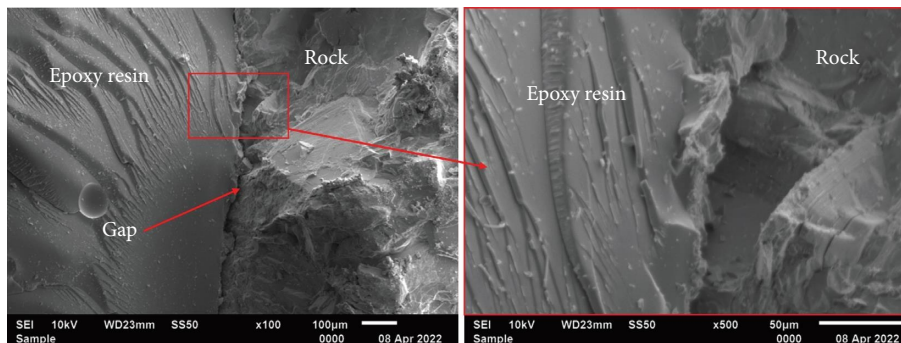


FIGURE 26: SEM image of the failed bond surface with 14 d of curing.

than that at day 14, within 66.03–73.36 MPa. For the 28 d samples, the samples repaired with epoxy resin have a much higher UCS and larger peak strains from 0.0063 to 0.0088, sometimes larger than that of intact rock, as described in Section 3.3, which is vital for cavern projects, making epoxy resin a desirable repair material for damage engineering [57].

3.4.2. *Repair with UPC.* Figure 29 shows the image before and after the failure of the samples repaired with UPC with a 14 d curing time and a 3 mm repair width. Figure 30 shows the damaged samples with 28 d of curing and 1 mm and 3 mm repair widths. In the case of the 3 mm repair width, the stone body on the fracture surface at day 28 is more complete than that at day 14.

Figure 31 shows that the UCS decreases with increasing repair width and that the UCS at day 28 is much larger than that at day 14. For samples with repair widths of 1 mm and 3 mm at day 28, the UCSs are 20.72 MPa and 16.27 MPa, respectively. The main reason for the results is that UPC is a brittle material, and its UCS is not high; thus, when the repair width increases, the material more easily undergoes shear damage. The UCS of the sample after 14 d of curing with a 3 mm width is only 7.48 MPa, which is partly due to the insufficient development of the repair material strength and bonding between the repair material and the rock surface.

3.5. *Comparison of the Effects on Strength Recovery.* From Section 3.2, the UCS of intact rock is 107.64 MPa. Figure 32

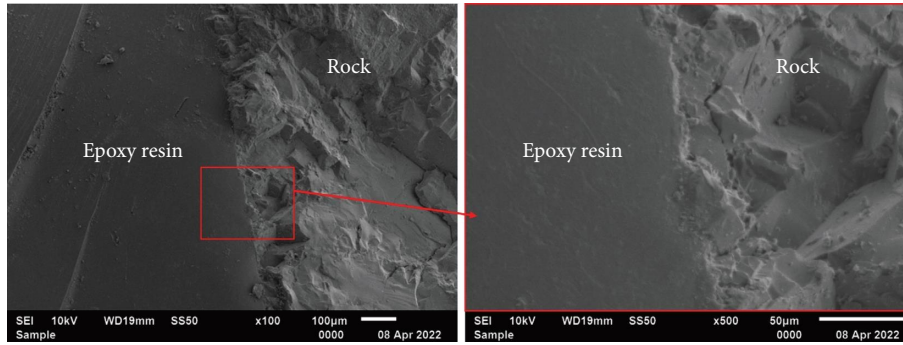


FIGURE 27: SEM image of the failed bond surface with 28 d of curing.

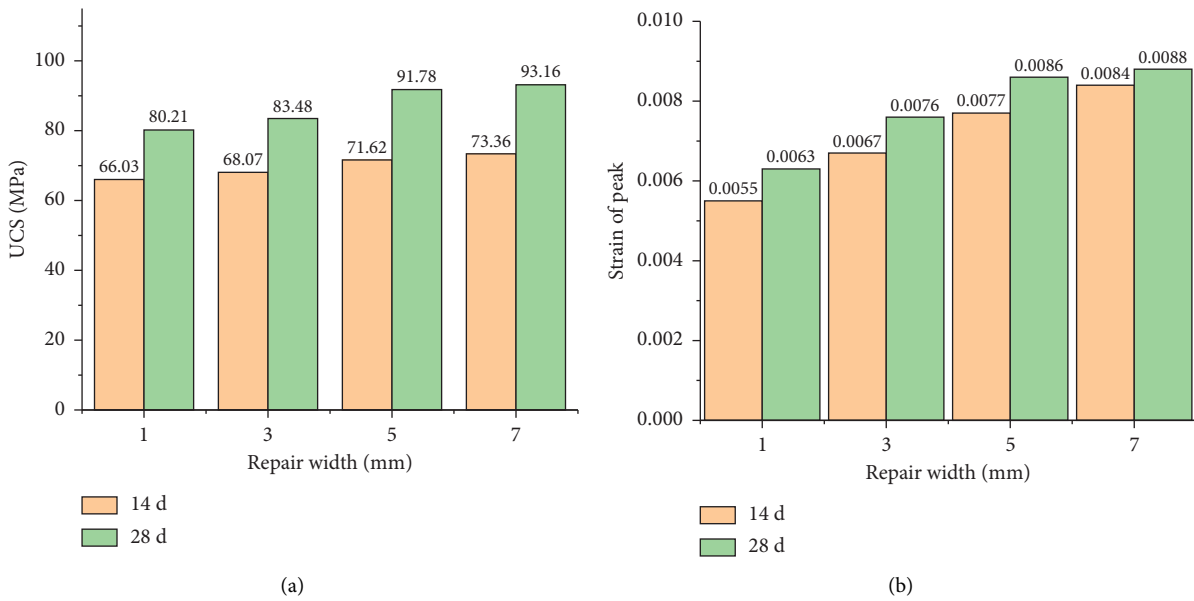


FIGURE 28: UCS (a) peak strain and (b) for different epoxy repair widths at days 14 and 28.

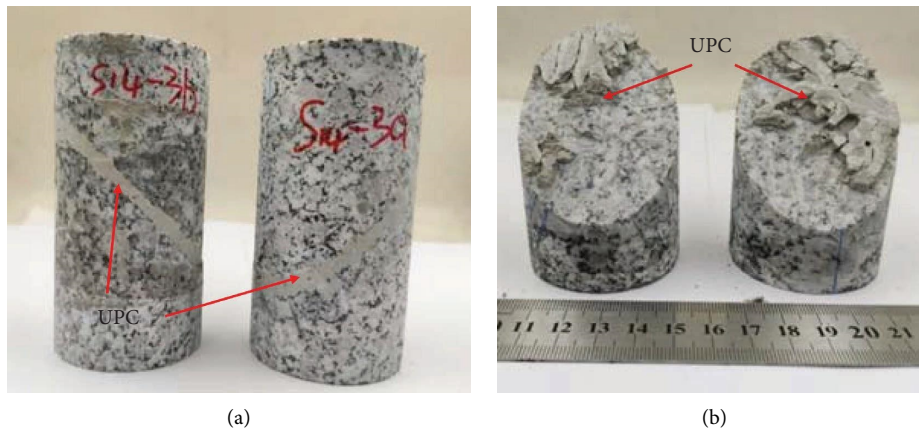


FIGURE 29: Before damage (a) after damage and (b) of the sample at day 14 with a 3 mm cement repair width.

shows the k_r of epoxy resin (14 d and 28 d) and UPC (14 d) as repair materials. Apparently, for epoxy resin, the effect on recovery increases as the repair width increases, and the k_r

(74.52–86.55%) at day 28 is clearly better than that (61.34–68.16%) at day 14; however, epoxy resin has an overwhelming advantage over UPC in both cases. For

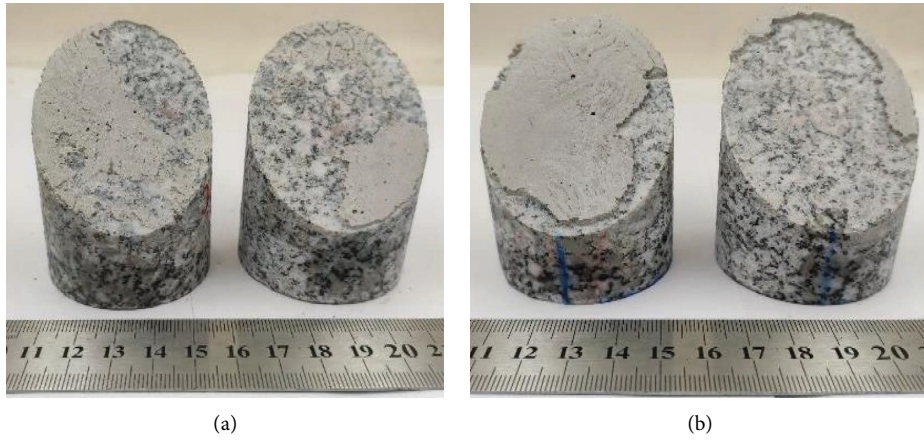


FIGURE 30: Damaged cement-repaired samples with different crack widths at day 28: 1 mm (a) and 3 mm (b).

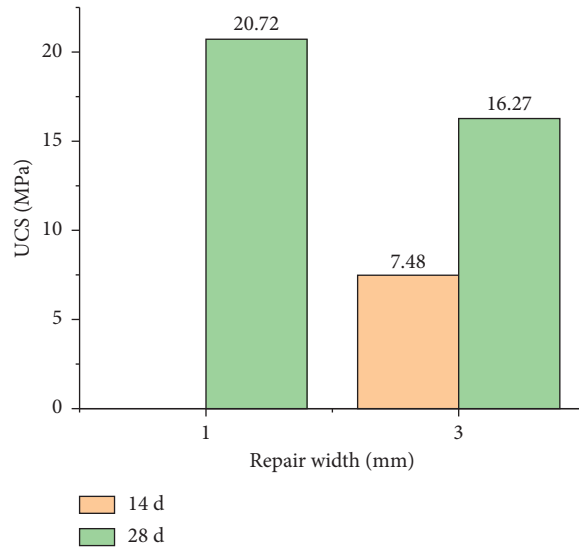


FIGURE 31: UCS of UPC-repaired samples with crack widths of 1 mm at day 14 and 1 mm and 3 mm at day 28.

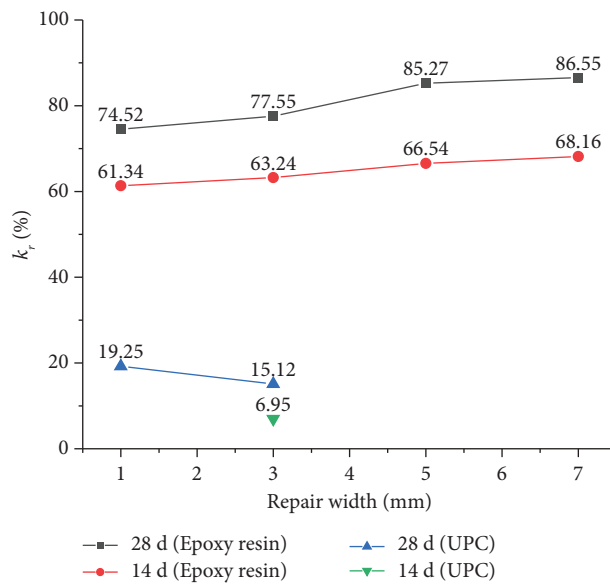


FIGURE 32: k_r of epoxy resin and UPC for cracked rock with different repair widths and curing times.

TABLE 2: UCS recovery listed in other references.

Ref	Bonding material/substrate	Curing time (d)	UCS (MPa)
[58]	Cement-based self-stress composite grouting material/coal body	14/28	10.89/12.1
[59]	Portland cement-based single slurry/limestone	14/91	Approximately 6.0/14.0
[60]	XH160 filling glue/rock	—	Approximately 50.0
[21]	Plain grout mortar/dry surface concrete	3/28	8.6/18.4
Present study	UPC/granite	14/28	6.95/15.12 (with a 3 mm wide crack)
Present study	Epoxy resin ($k_{CE}=0.25$, $k_A=0.01$)/granite	14/28	63.24/77.55 (with a 3 mm wide crack)

instance, with a 3 mm wide crack, the k_r values of epoxy resin on days 14 and 28 are 63.24% and 77.55%, respectively, while the k_r values of UPC are only 6.95% and 15.12%, respectively. Notably, k_r decreases with increasing crack width for UPC-repaired samples.

Moreover, compared to the strengths listed in other references, as shown in Table 2, and the UPC materials in this paper, the strength effect has an absolute advantage.

Therefore, compared with UPC and other repair materials, epoxy resin is a promising repair material with a good effect on strength recovery. Additionally, the effect on strength recovery is closely related to the repair material, curing time, and crack width.

4. Conclusions

This paper mainly explored the UCS of epoxy resin and UPC stone bodies and their effects on the strength recovery of granite samples with artificial cracks of various widths. The influence of temperature and k_A on the viscosity of epoxy resin was tested, and the impact of k_{CE} , k_A and stirring mode on the strength was considered. The UCS test on the repaired samples also considered the effect of the curing time. With the self-designed grouting repair device, the selected epoxy resin and UPC ingredients were used to repair rock with cracks of various widths, and the effect on recovery was evaluated by k_r . The following conclusions can be made:

- (1) The viscosity of epoxy resin decreases with increasing temperature and the addition of ethanol.
- (2) The UCS of epoxy resin of 92.41 MPa with vacuum stirring is larger than that of 75.88 MPa with air mixing because there are fewer bubbles in the material stirred under vacuum than in that stirred in the air. The UCS of epoxy resin is significantly better than that of UPC, and moreover, epoxy resin has a much larger peak strain.
- (3) k_{CE} affects the strength of the sample, and the maximum UCS value is 92.41 MPa with a k_{CE} value of 0.25. k_A can affect the UCS of epoxy resin, with the UCS reaching the maximum value of 94.65 MPa when k_A is 0.01.
- (4) Epoxy resin has a distinctly better effect on strength recovery than UPC. For instance, with a repair width of 3 mm, the UCS of epoxy resin at day 28 is 83.48 MPa, while that of UPC is only 20.72 MPa.
- (5) The UCS of the samples with different crack widths repaired by epoxy resin varies. With increasing crack

width, k_r increases from 74.52% to 86.55% for the 28 d samples, while k_r is only 15.12–19.25% with UPC repair. The effect on recovery improves for epoxy resin repaired samples, which is contrary to the trend for UPC.

Overall, epoxy resin has high strength, a low elastic modulus, and excellent ductility, showing promising applicability in rock engineering as a repair material to bond rock fractures and withstand large deformations.

Data Availability

The data used to support the findings of this study are included within the article.

Conflicts of Interest

The authors declare that they have no conflicts of interest.

Authors' Contributions

Yaming Zhou performed data curation and wrote the original draft. Jianhai Zhang conceptualized the study, performed methodology, provided the resources, performed supervision, and was involved in funding acquisition. Ru Zhang was involved in funding acquisition and performed experimental aid. Enlong Liu performed investigation. Lu Wang supervised the study. Guoyan Zhang performed experimental aid.

Acknowledgments

The authors acknowledge the financial support from the National Natural Science Foundation of China (Grant no. U1965203) and “The Research on Support Time and Deformation Warning of Surrounding Rock of Large Underground Cavern Group under Extremely High Stress condition of Shuangjiangkou Hydropower” (Grant no. A147 SG). The authors would also like thank Dr. Yang Liu and Dr. Zhaopeng Zhang from the Key Laboratory of Deep Earth Science and Engineering (Ministry of Education) at Sichuan University for their meaningful discussions and assistance with experiments in this work.

References

- [1] Y. Lu, M. He, L. Wang, B. Ren, X. Sun, and K. Zhang, “In-situ visualization experiments on the microscopic process of particle filtration of cement grouts within a rock fracture,”

- Tunnelling and Underground Space Technology*, vol. 95, Article ID 103157, 2020.
- [2] X. Chen, L. Chen, B. Ma et al., "Mechanical-characteristic evaluation of excavation unloading rock mass subject to high-temperature conditions," *Engineering Failure Analysis*, vol. 130, Article ID 105757, 2021.
 - [3] A. Abolhasani, M. Shakouri, M. Dehestani, B. Samali, and S. Banihashemi, "A comprehensive evaluation of fracture toughness, fracture energy, flexural strength and micro-structure of calcium aluminate cement concrete exposed to high temperatures," *Engineering Fracture Mechanics*, vol. 261, Article ID 108221, 2022.
 - [4] L. Kong, P. G. Ranjith, Q. B. Li, and Y. Song, "Rock grain-scale mechanical properties influencing hydraulic fracturing using Hydro-GBM approach," *Engineering Fracture Mechanics*, vol. 262, Article ID 108227, 2022.
 - [5] S. A. Altoubat and D. A. Lange, "Creep, shrinkage, and cracking of restrained concrete at early age," *ACI Materials Journal*, vol. 98, pp. 323–331, 2001.
 - [6] F. L. Gea dos Santos and T. L. D. Forti, "Concrete cohesive curves for specimens with different sizes: a study of inverse analysis and size effect," *Engineering Fracture Mechanics*, vol. 261, Article ID 108249, 2022.
 - [7] X. Liu, Z. Zhu, and A. Liu, "Permeability characteristic and failure behavior of filled cracked rock in the triaxial seepage experiment," *Advances in Civil Engineering*, vol. 2019, Article ID 3591629, 12 pages, 2019.
 - [8] B. Gonçalves da Silva and H. Einstein, "Physical processes involved in the laboratory hydraulic fracturing of granite: visual observations and interpretation," *Engineering Fracture Mechanics*, vol. 191, pp. 125–142, 2018.
 - [9] Y.-S. Wang, K.-D. Peng, Y. Alrefaei, and J.-G. Dai, "The bond between geopolymer repair mortars and OPC concrete substrate: strength and microscopic interactions," *Cement and Concrete Composites*, vol. 119, Article ID 103991, 2021.
 - [10] X. Fan, R. Chen, H. Lin, H. Lai, C. Zhang, and Q. Zhao, "Cracking and failure in rock specimen containing combined flaw and hole under uniaxial compression," *Advances in Civil Engineering*, vol. 2018, Article ID 9818250, 15 pages, 2018.
 - [11] M. R. Azadi, A. Taghichian, and A. Taheri, "Optimization of cement-based grouts using chemical additives," *Journal of Rock Mechanics and Geotechnical Engineering*, vol. 9, no. 4, pp. 623–637, 2017.
 - [12] W. Zhang, S. Li, J. Wei et al., "Grouting rock fractures with cement and sodium silicate grout," *Carbonates and Evaporites*, vol. 33, no. 2, pp. 211–222, 2018.
 - [13] D. Zhou, Z. Zhao, B. Li, Y. Chen, and W. Ding, "Permeability evolution of grout infilled fractures subjected to triaxial compression with low confining pressure," *Tunnelling and Underground Space Technology*, vol. 104, Article ID 103539, 2020.
 - [14] X. Liu, F. Wang, J. Huang, S. Wang, Z. Zhang, and K. Nawnit, "Grout diffusion in silty fine sand stratum with high groundwater level for tunnel construction," *Tunnelling and Underground Space Technology*, vol. 93, Article ID 103051, 2019.
 - [15] X. Du, H. Fang, S. Wang, B. Xue, and F. Wang, "Experimental and practical investigation of the sealing efficiency of cement grouting in tortuous fractures with flowing water," *Tunnelling and Underground Space Technology*, vol. 108, Article ID 103693, 2021.
 - [16] H. Güllü, "Factorial experimental approach for effective dosage rate of stabilizer: application for fine-grained soil treated with bottom ash," *Soils and Foundations*, vol. 54, no. 3, pp. 462–477, 2014.
 - [17] C. R. Gagg, "Cement and concrete as an engineering material: an historic appraisal and case study analysis," *Engineering Failure Analysis*, vol. 40, pp. 114–140, 2014.
 - [18] Y. Tian, Q. Liu, H. Ma, Q. Liu, and P. Deng, "New peak shear strength model for cement filled rock joints," *Engineering Geology*, vol. 233, pp. 269–280, 2018.
 - [19] M. Rahman, J. Wiklund, R. Kotzé, and U. Håkansson, "Yield stress of cement grouts," *Tunnelling and Underground Space Technology*, vol. 61, pp. 50–60, 2017.
 - [20] Y.-J. Wang, Z.-M. Wu, J.-J. Zheng, and X.-M. Zhou, "3D analytical investigation on the overall pullout behavior of grouted anchorages in presence of shear failure of grout," *Engineering Failure Analysis*, vol. 109, Article ID 104249, 2020.
 - [21] A. Sharkawi, M. Taman, H. M. Afefy, and Y. Hegazy, "Efficiency of geopolymer vs. high-strength grout as repairing material for reinforced cementitious elements," *Structures*, vol. 27, pp. 330–342, 2020.
 - [22] A. Albidah, A. Abadel, F. Alrshoudi, A. Altheeb, H. Abbas, and Y. Al-Salloum, "Bond strength between concrete substrate and metakaolin geopolymer repair mortars at ambient and elevated temperatures," *Journal of Materials Research and Technology*, vol. 9, no. 5, Article ID 10732, 2020.
 - [23] S.-Y. Guo, X. Zhang, J.-Z. Chen et al., "Mechanical and interface bonding properties of epoxy resin reinforced Portland cement repairing mortar," *Construction and Building Materials*, vol. 264, Article ID 120715, 2020.
 - [24] M. Akiyama and S. Kawasaki, "Novel grout material comprised of calcium phosphate compounds: in vitro evaluation of crystal precipitation and strength reinforcement," *Engineering Geology*, vol. 125, pp. 119–128, 2012.
 - [25] C. Butrón, M. Axelsson, and G. Gustafson, "Silica sol for rock grouting: laboratory testing of strength, fracture behaviour and hydraulic conductivity," *Tunnelling and Underground Space Technology*, vol. 24, no. 6, pp. 603–607, 2009.
 - [26] Y. Wang, C. Wang, S. Zhou, and K. Liu, "Influence of cationic epoxy resin type on electrophoretic deposition effect on repair of rust-cracked reinforced concrete," *Construction and Building Materials*, vol. 324, Article ID 126714, 2022.
 - [27] A. Draganović and H. Stille, "Filtration and penetrability of cement-based grout: study performed with a short slot," *Tunnelling and Underground Space Technology*, vol. 26, no. 4, pp. 548–559, 2011.
 - [28] O. Saeidi, H. Stille, and S. R. Torabi, "Numerical and analytical analyses of the effects of different joint and grout properties on the rock mass groutability," *Tunnelling and Underground Space Technology*, vol. 38, pp. 11–25, 2013.
 - [29] J. Rafi and H. Stille, "A method for determining grouting pressure and stop criteria to control grout spread distance and fracture dilation," *Tunnelling and Underground Space Technology*, vol. 112, Article ID 103885, 2021.
 - [30] N. Aziz, D. Majoor, and A. Mirzaghorbanali, "Strength properties of grout for strata reinforcement," *Procedia Engineering*, vol. 191, pp. 1178–1184, 2017.
 - [31] M. Sharghi, H. Chakeri, and Y. Ozcelik, "Investigation into the effects of two component grout properties on surface settlements," *Tunnelling and Underground Space Technology*, vol. 63, pp. 205–216, 2017.
 - [32] Z. Zhou, D. Gao, G. Lin, and W. Sun, "Static and dynamic mechanical properties of epoxy nanocomposites reinforced by hybridization with carbon nanofibers and block ionomers,"

- Engineering Fracture Mechanics*, vol. 271, Article ID 108638, 2022.
- [33] P. Ghassemi and V. Toufigh, "Durability of epoxy polymer and ordinary cement concrete in aggressive environments," *Construction and Building Materials*, vol. 234, Article ID 117887, 2020.
- [34] A. M. López-Buendía, C. Guillem, J. M. Cuevas, F. Mateos, and M. Montoto, "Natural stone reinforcement of discontinuities with resin for industrial processing," *Engineering Geology*, vol. 166, pp. 39–51, 2013.
- [35] M. Axelsson and G. Gustafson, "A robust method to determine the shear strength of cement-based injection grouts in the field," *Tunnelling and Underground Space Technology*, vol. 21, no. 5, pp. 499–503, 2006.
- [36] Y. He, X. Zhang, R. D. Hooton, and X. Zhang, "Effects of interface roughness and interface adhesion on new-to-old concrete bonding," *Construction and Building Materials*, vol. 151, pp. 582–590, 2017.
- [37] W. Song, F. Xu, H. Wu, and Z. Xu, "Laboratory investigation of the bonding performance between open-graded friction course and underlying layer," *Engineering Fracture Mechanics*, vol. 265, Article ID 108314, 2022.
- [38] Z. Li, B. Nocelli, and S. Saydam, "Effect of rock strength and surface roughness on adhesion strength of thin spray-on liners," *International Journal of Rock Mechanics and Mining Sciences*, vol. 91, pp. 195–202, 2017.
- [39] B. Zhang, S. Li, K. Xia et al., "Reinforcement of rock mass with cross-flaws using rock bolt," *Tunnelling and Underground Space Technology*, vol. 51, pp. 346–353, 2016.
- [40] Z. Zhou, X. Cai, X. Du, S. Wang, D. Ma, and H. Zang, "Strength and filtration stability of cement grouts in porous media," *Tunnelling and Underground Space Technology*, vol. 89, pp. 1–9, 2019.
- [41] Y. Guo, C. Yang, L. Wang, and F. Xu, "Effects of cyclic loading on the mechanical properties of mature bedding shale," *Advances in Civil Engineering*, vol. 2018, Article ID 8985973, 9 pages, 2018.
- [42] W. Sui, J. Liu, W. Hu, J. Qi, and K. Zhan, "Experimental investigation on sealing efficiency of chemical grouting in rock fracture with flowing water," *Tunnelling and Underground Space Technology*, vol. 50, pp. 239–249, 2015.
- [43] P. Li, Q. S. Zhang, S. C. Li, and X. Zhang, "Time-dependent empirical model for fracture propagation in soil grouting," *Tunnelling and Underground Space Technology*, vol. 94, Article ID 103130, 2019.
- [44] L. Weng, Z. Wu, S. Zhang, Q. Liu, and Z. Chu, "Real-time characterization of the grouting diffusion process in fractured sandstone based on the low-field nuclear magnetic resonance technique," *International Journal of Rock Mechanics and Mining Sciences*, vol. 152, Article ID 105060, 2022.
- [45] Z. Zhong, R. Deng, J. Zhang, and X. Hu, "Fracture properties of jointed rock infilled with mortar under uniaxial compression," *Engineering Fracture Mechanics*, vol. 228, Article ID 106822, 2020.
- [46] H. Li, Z. Yang, and H. Li, "Mechanical characteristics and failure mechanism of siltstone with different joint thickness," *Advances in Civil Engineering*, vol. 2020, pp. 1–10, 2020.
- [47] J. Funehag and J. Thörn, "Radial penetration of cementitious grout – laboratory verification of grout spread in a fracture model," *Tunnelling and Underground Space Technology*, vol. 72, pp. 228–232, 2018.
- [48] P. Yang, Y.-H. Liu, S.-W. Gao, and S. Xue, "Experimental investigation on the diffusion of carbon fibre composite grouts in rough fractures with flowing water," *Tunnelling and Underground Space Technology*, vol. 95, Article ID 103146, 2020.
- [49] H. Zhao, T. Ren, and A. Remennikov, "Standing support incorporating FRP and high water-content material for underground space," *Tunnelling and Underground Space Technology*, vol. 110, Article ID 103809, 2021.
- [50] B. Bohloli, E. K. Morgan, E. Grøv, O. Skjølsvold, and H. O. Hognestad, "Strength and filtration stability of cement grouts at room and true tunnelling temperatures," *Tunnelling and Underground Space Technology*, vol. 71, pp. 193–200, 2018.
- [51] J. C. Zelanko and M. G. Karfakis, "Development of a polyester-based pumpable grout," *International Journal of Rock Mechanics and Mining Sciences*, vol. 34, no. 3-4, Article ID 357.e1, 1997.
- [52] C. A. Anagnostopoulos, "Laboratory study of an injected granular soil with polymer grouts," *Tunnelling and Underground Space Technology*, vol. 20, no. 6, pp. 525–533, 2005.
- [53] R. Šňupárek and K. Souček, "Laboratory testing of chemical grouts," *Tunnelling and Underground Space Technology*, vol. 15, no. 2, pp. 175–185, 2000.
- [54] S. Smaniotto, M. Neuner, A. Dummer, T. Cordes, and G. Hofstetter, "Experimental study of a wet mix shotcrete for primary tunnel linings—Part I: evolution of strength, stiffness and ductility," *Engineering Fracture Mechanics*, vol. 267, Article ID 108409, 2022.
- [55] Q. Ma, Q. Su, and P. Yuan, "Dynamic behavior and energy evolution characteristic of Deep roadway sandstone containing weakly filled joint at various angles," *Advances in Civil Engineering*, vol. 2020, Article ID 8817107, 12 pages, 2020.
- [56] B. Bohloli, O. Skjølsvold, H. Justnes, R. Olsson, E. Grøv, and A. Aarset, "Cements for tunnel grouting – rheology and flow properties tested at different temperatures," *Tunnelling and Underground Space Technology*, vol. 91, Article ID 103011, 2019.
- [57] J. R. Lester, A. G. Brown, and J. M. Ingham, "Stabilisation of the cathedral of the blessed sacrament following the canterbury earthquakes," *Engineering Failure Analysis*, vol. 34, pp. 648–669, 2013.
- [58] J. P. Zhang, L. M. Liu, Q. H. Li et al., "Development of cement-based self-stress composite grouting material for reinforcing rock mass and engineering application," *Construction and Building Materials*, vol. 201, pp. 314–327, 2019.
- [59] F. Sha, C. Lin, Z. Li, and R. Liu, "Reinforcement simulation of water-rich and broken rock with Portland cement-based grout," *Construction and Building Materials*, vol. 221, pp. 292–300, 2019.
- [60] A. Jin, Z. Wang, and S. J. C. J. R. M. Ming, "Engineering," *Experimental Investigation on Mechanical Property of Reinforced Fractured Rock*, vol. 31, no. 1, 2012.